

Investigation of Exotic Nuclear Shapes and its Evolution using a Large Compton Suppressed Clover Array

R. Palit*

*Department of Nuclear and Atomic Physics,
Tata Institute of Fundamental Research, Mumbai - 400005, INDIA*

Nuclear landscape around $A \sim 110$ and $A \sim 130$ are the regions where the interplay between single-particle, vibrational and rotational degrees of excitation modes has generated a rich variety of nuclear structure phenomena. New high-spin spectroscopic data on nuclei in these regions are presented which highlights different aspects of degenerate dipole bands, gamma vibrational bands, magnetic rotations and isomers. Scope of production of transitional nuclei at medium spin with Li, Be and B induced reactions for horizontal spectroscopic study is highlighted. The perspectives offered by the forthcoming operation of the clover array coupled to a new digital data acquisition system are discussed briefly.

1. Introduction

A basic property of the nucleus is its geometrical shape which is result of the delicate balance between the shell structure and the residual interactions between the nucleons. Investigation of the effect of varying rotational stress on nucleus continues to provide new insights on the symmetry of the nuclear systems involving its shape, and the angular momenta of valance nucleons and the collective rotation. Recently, the nuclei in $A \sim 110$ and $A \sim 130$ regions have attracted much attention for investigation of high spin phenomena related with chiral rotations, magnetic rotations, gamma vibrations and its coupling with rotational modes. High-spin band structure in this mass region has been experimentally investigated through heavy ion induced reactions (see, for example, refs. [1–11]). Along with these studies many low-lying non-yrast states have also been investigated in the β -decay spectroscopic methods [12] and Coulomb excitations of stable as well as radioactive ions [13–15]. Nuclei in this mass region depict a variety of band structure which are built on different excitation modes. The excited states for the neutron deficient nuclei around $A \sim 110$ involve proton holes and

neutron particles and that for nuclei around $A \sim 130$ have proton particles and neutron holes in high- j orbitals. Depending upon the coupling of the angular momenta of valance neutrons and protons with that of the even-even core different types of excitations [16–18], namely, magnetic rotation, chiral twin bands and recently predicted chopstick configurations have been discussed for these nuclei.

In the present paper, we report on our work on the high spin states of odd-odd In isotopes in $A \sim 110$ and Cs and Ce isotopes in $A \sim 130$ with neutron number below $N=82$ shell gap. Along with heavy ion induced fusion reactions involving beams like $^{16,18}\text{O}$ to ^{32}S , incomplete fusion reactions are explored to study the yield of the high spin states of nuclei near the line of stability. For the incomplete fusion (ICF) reactions, projectiles like Li, Be and B having cluster structure of alpha + core have been taken. In this connection, we will describe the perspective offered by the forthcoming operations of the clover array and ancillary detectors coupled to a new digital data acquisition system for exploring the spin-excitation energy surface of nuclei using different reactions.

*Electronic address: palit@tifr.res.in

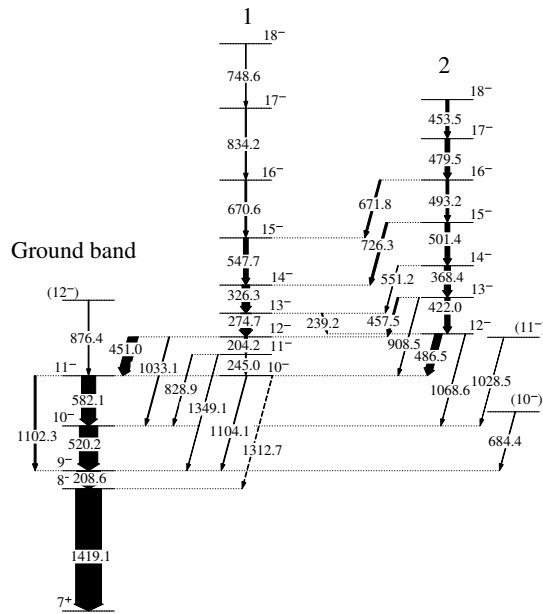


FIG. 1: The partial level scheme of ^{106}In developed in the present work.

2. Experimental Results on Regular Sequence of Dipole Bands in odd-odd In isotopes

Regular sequences of M1 transitions are observed for $56 < N < 62$ in $A \approx 110$ region, but gradually disappear with decreasing neutron number. Doublet dipole bands are known in odd-odd Rh and Ag isotopes, not much is known in In isotopes [19]. Tri-axial relativistic mean field calculations indicate multiple chiral rotations in $A \sim 110$ region [20]. In order to understand the nature of the magnetic dipole bands and search for chiral rotations, a systematic investigation of odd-odd In isotopes are carried out [7, 11, 21].

High spin states in ^{106}In were populated using $^{78}\text{Se}(^{32}\text{S}, p3n)$ reaction at 125-MeV with a target consisted of 1 mg/cm^2 of ^{78}Se deposited on gold backing. The experiment was performed at TIFR-BARC Pelletron Linac Facility (PLF) at Mumbai. An array of seven Compton suppressed clover detectors was used to measure the gamma rays. The clover de-

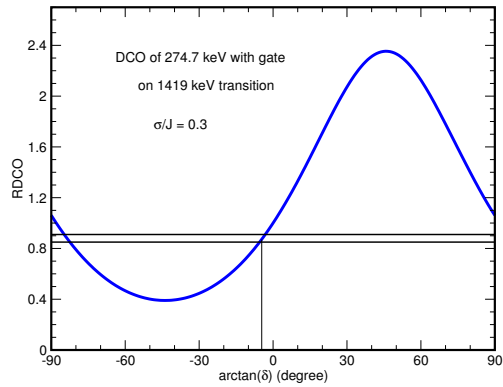


FIG. 2: The variation of RDCO value with the mixing ratio for 274 keV transition and extraction of mixing ratio.

ectors were arranged in the horizontal plane at 150° , 120° , 30° , 30° , 60° , 100° and 150° with respect to the beam direction. The data were acquired when at least two clover detectors and two NaI(Tl) fired simultaneously.

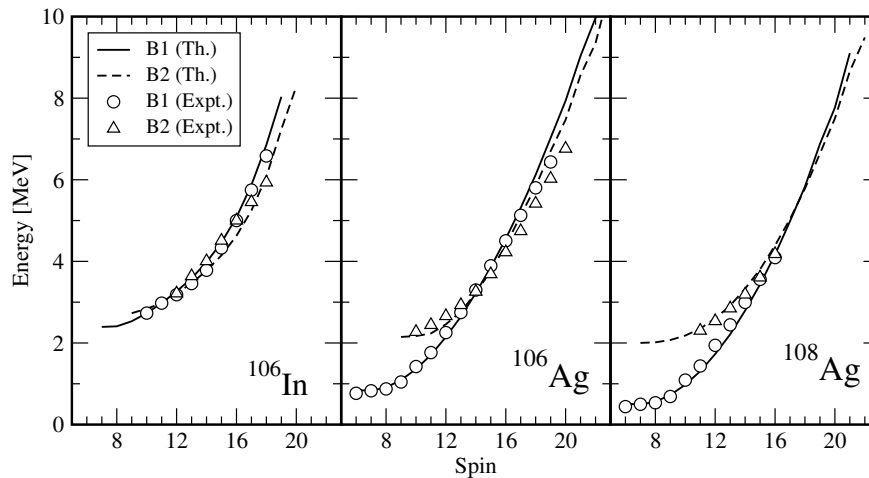


FIG. 3: Comparison of the energy levels of the negative parity degenerate bands with the PHF calculations based on different configurations for ^{106}In , ^{106}Ag and ^{108}Ag isotopes.

The Directional Correlation of Oriented states (DCO) and the integrated polarization direction correlation (IPDCO) analysis were carried out to determine the spin and parity of different states. Around forty new transitions comprising of three new band structures and low lying irregular excitations were established [7]. Part of the present level scheme is shown in Fig. 1 depicting the degenerate dipole bands.

Ground band based on 8^- state was extended up to 12^- with the addition of the top most transition with energy 876.4 keV. Our work suggests that the 274.7, 326.3, 547.7, 670.6, 834.2 and 748.6 keV transitions form a part of another band with 10^- band-head at ~ 2.7 MeV. This is confirmed with the observation of multiple out feeding transitions with energies, 204.2, 245.0, 828.9, 1104.1 and 1349.1 keV from the various levels of the band 2. Further, the mixing ratio analysis was carried out for the lower dipole transitions of bands 2 and 3, viz, 274.7, 326.3, 422.0, and 368.4, from their extracted R_{DCO} values with gate on 208.6 keV pure $\Delta I = 1$ transition. The R_{DCO} ratios suggest that these γ -rays to have a small mixing ratio $-7^0 < \arctan(\delta) < -1^0$. The variation of the R_{DCO} ratio of 274.7

keV transition with mixing ratio for 1419 keV gated transition is shown in Fig. 2. The measured R_{DCO} ratio of 274.7 keV transition indicates a small mixing ratio for this transition. Similar analysis along with the IPDCO measurements suggest pure M1 nature for the 326.3, 422.0, and 368.4 keV intra-band $\Delta I = 1$ transitions.

PHF calculations, used to understand the configurations involved in the observed doublet bands in ^{106}In , is based on Hamiltonian that consists of the single particle and two-body interaction terms [22]. ^{90}Zr is taken as the core in the present HF calculations. Axial symmetry of the Hartree-Fock field is assumed in the calculation. The intrinsic configurations $|\phi_K\rangle$ used in the present calculations for bands 1 and 2 are $\pi g_{9/2}(9/2^+) \otimes \nu h_{11/2}(1/2^-)(g_{7/2})^2$ with $K^\pi = 5^-$ and $\pi g_{9/2}(7/2^+) \otimes \nu h_{11/2}(1/2^-)(g_{7/2})^2$ with $K^\pi = 4^-$, respectively. The I-projection states based on these configurations have been plotted in Fig. 3 along with the experimental level energies. The excitation energy of the lowest $I^\pi = 10^-$ state in band 1 and that of the lowest $I^\pi = 12^-$ state in band 2 have been normalized to experimental excitation energies for the ease of comparison of level ener-

gies. The relative level spacing in these two bands are reproduced in the calculations. The calculated B(M1)/B(E2) transition strengths in these two bands are found to be large ($\geq 40 (\mu_N/eb)^2$). This is in favor of the fact that no cross-over E2 transitions have been identified. Though the presence of the inter-band transitions indicate some mixing between bands 1 and 2, the upper limit of the mixing matrix element is found to be as low as 0.5 keV due to the nearly degenerate 16^- states of bands 1 and 2. In $^{106,108}\text{Ag}$ isotopes, a pair of dipole bands have been reported in Ref. [23, 24]. PHF calculations are performed for these Ag isotopes to assign the configurations of these dipole bands and have the systematics of these structures. The HF prolate mean field is favoured for both $^{106,108}\text{Ag}$ isotopes with $\beta = 0.15$. The configurations used for the two dipole bands in these odd-odd Ag isotopes are $\pi g_{9/2}(7/2^+) \otimes \nu h_{11/2}(1/2^-)(g_{7/2})^2$ with $K^\pi = 4^-$ and $\pi g_{9/2}(9/2^+) \otimes \nu h_{11/2}(1/2^-)(g_{7/2})^2$ with $K^\pi = 5^-$, respectively. The angular momentum projected states based on these configurations fairly reproduce the measured level spacing of the dipole bands as shown in Fig. 3. The B(M1)/B(E2) ratios were calculated as a function of spin for these bands based on the above configurations and agree with the measured values. This provides additional support for the assigned configurations for the pair of dipole bands in $^{106,108}\text{Ag}$ isotopes.

The excited states of ^{112}In were populated through $^{100}\text{Mo}(^{16}\text{O}, p3n)$ reaction at 85 MeV beam energy and gamma rays were measured with 18 CS-clover detector array at IUAC, New Delhi. Polarization and lifetime measurements have been carried out for the excited states of ^{112}In . The B(M1) transition strengths in the strongly populated dipole band with gamma ray sequence of 128 - 178 - 272 - 393 - 554 - 708 - 738 keV are measured with Doppler Shift Attenuation Method (DSAM) technique and decrease with increasing spin. The typical lineshape observed for 393 keV transition in the clover detectors, kept at 148° with respect to beam direction, is shown in Fig. 4(a). Polarization measurements confirm the positive parity of

the bandhead and M1 nature of the intra band transitions. A quasi-particle configuration $\pi g_{9/2} \times \nu((h_{11/2})^2 d_{5/2}/g_{7/2})$ is used in the tilted axis cranking (TAC) calculation for the dipole band. A minimum is found at deformation of $\epsilon_2 = 0.12$ and $\gamma = 6^\circ$. The extracted B(M1) strengths show a decreasing trend with increasing spin (as shown in Fig 4(b)) and thereby confirms the shears mechanism proposed for generation of angular momentum in this band [25].

3. Gamma vibrations and its Coupling with Rotations in $A \sim 130$ region

The issue of stable triaxial nuclear shape is one which has been debated for decades in nuclear structure studies. Level structure of the gamma vibrational bands and the associated transition strengths give crucial information about the nature of triaxiality of the nuclei. While some of the even-even nuclei in $A \sim 130$ region are interpreted to have gamma soft behavior [26], the odd-odd and even-odd nuclei require a rigid triaxial even-even core to support the observed chiral bands [18, 27, 28]. A systematic comparison of the gamma bands of even-even nuclei with that of the nearby even-odd or odd-even nuclei will be worthwhile to study the effect of the valance particle on the triaxiality of the even-even core. In our measurement, two bands, namely, B1 and B9 have been observed for the first time [6]. The decay pattern of the band B9, with bandhead spin of $I^\pi = 15/2^-$, is found to be quite similar to that of the gamma vibrational band built on the favored signature of the $\pi h_{11/2}$ band in lighter Cs isotopes (see Ref. listed in [6]). It will be interesting to experimentally identify the states of gamma vibrational band with intermediate spins $I^\pi = 17/2^-, 21/2^-, \text{etc.}$ The excited states of B1 band decay to the B5 band via the $\Delta I = 1$ transitions having energy higher than 1 MeV and it has been identified as the gamma band coupled with the $\pi g_{7/2}$ orbital. Similar band structure has not been observed in neighboring odd Cs isotopes. The gamma band coupled with $\pi g_{7/2}$ orbital should have the bandhead spin of $I^\pi = 11/2^+$.

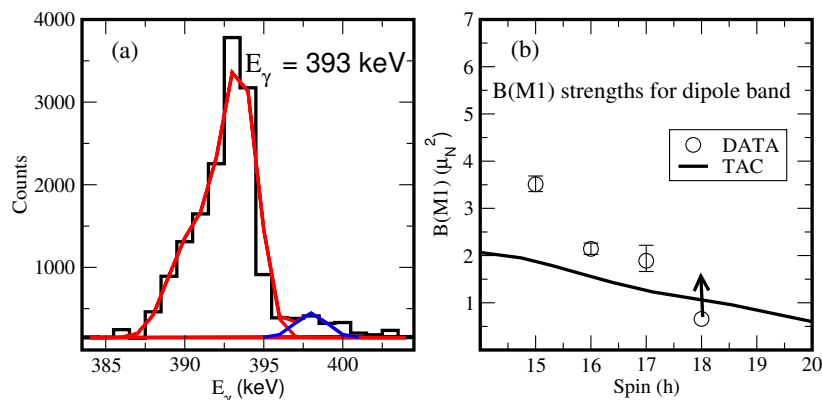


FIG. 4: (a) Lineshape of 393 keV transition observed at 148° detector and (b) Plot of B(M1) vs spin for B3 band of ¹¹²In along with TAC calculation.

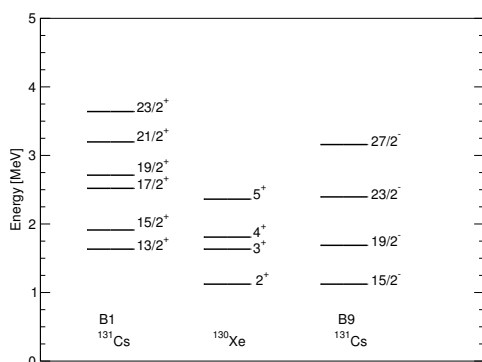


FIG. 5: Comparison of the relative spacing of the experimental levels in gamma bands B1 and B9 of ¹³¹Cs with that of neighboring ¹³⁰Xe nucleus. Spins of the different states are marked for each band. The lowest observed states of all these gamma bands are normalized as explained in the text.

The lowest energy state observed in this band has a spin $I^\pi = 13/2^+$. For comparison of the relative level spacings of B1 and B9 bands with that of the gamma band of neighbouring even-even nucleus ¹³⁰Xe [29], the 13/2⁺ state of B1 and 15/2⁺ state of B9 band have been normalized to 3⁺ and 2⁺ states of the gamma band in ¹³⁰Xe, respectively (see Fig. 5). The B1 gamma band built on the $\pi g_{7/2}$ seems to have the same staggering pattern as that of

gamma band in ¹³⁰Xe. Similar comparison for B9 band is not possible for the time being as the intermediate levels are not yet identified. Another negative parity band B15 has been found in the present work, which is having a similar level spacing and feeding pattern to the favored signature of the $\pi h_{11/2}$ band as that of B9 band. More systematic is required to understand its structure.

The even-even Ce isotopes are interesting examples for the investigation of the coupling of gamma vibration and rotational modes which gives rise to interesting high spin phenomena. In this context, the partial level structure of ¹³⁴Ce developed in our recent measurement is shown in Fig. 6. The level structure shows the ground state and gamma vibrational bands up to $J^\pi = 26^+$ and 18^+ , respectively. The lowest two $I=10^+$ states have been identified long before experimentally in this nucleus and there has been a long standing puzzle regarding the structure of these two 10^+ states. The magnetic moments of both these states have been measured and it has been found that both these states have negative g-factors [31]. Thus indicating that both the 10^+ states have neutron structure and it was impossible to explain using any of the existing models. Triaxial projected shell model has been used for the understanding of the properties of this rotating gamma soft nucleus

tially to the total cross section. An experiment was performed to measure the contributions of different channels for the total reaction cross sections involving ${}^9\text{Be}$ experiment. This will be useful for optimization of the channel selection device for the identification of charged particle channels involving these projectiles. The experiment was performed using the ${}^9\text{Be}$ beam at energies $E_{beam} = 26 - 38$ MeV in steps of 1 MeV, from the 14UD TIFR-BARC Pelletron accelerator, Mumbai. The target ${}^{124}\text{Sn}$ of thickness 2.47 ± 0.04 mg/cm², which was measured using the Rutherford backscattering method, was used. Two Compton suppressed Clover detectors were kept at 125° and 90° with respect to the beam direction. Two charged particle detector telescopes and one monitor detector were placed at 65°, 160° and 30°, respectively. The gamma rays from the residues were identified in the clover detectors at 125°. A typical gamma ray adback spectrum from the clover detector at 125° and $E_{beam} = 38$ MeV is shown in Fig 8. The gamma ray lines from the evaporation residues following CF and ICF are identified and labeled. Emission cross sections of γ transitions decaying the lower states of even-even residues have been extracted using the measured photo-peak efficiency of the clover detector and the elastic scattered beam in the monitor. The γ -ray cross sections $\sigma_\gamma(J)$ for various transitions of the ground state band was plotted as a function of J and it was extrapolated up to $J = 0$ to get the corresponding ER cross section. For the odd-mass ${}^{129}\text{Xe}$, the cross sections were obtained using the measured intensities of the $\frac{11}{2}^-$ state at 587 keV and normalizing them with the $4n$ channel from the statistical model code PACE. These experimental ER cross sections are shown in Fig. 9. Open triangles correspond to cross sections for the formation of ${}^{126}\text{Te}(\text{ICF}; \alpha, 2n)$. Above the Coulomb barrier energies, the measured CF cross sections were found to be suppressed by a factor of $28 \pm 5\%$ compared to the coupled channel calculations[32]. The loss of flux causing the suppression of CF will be due to the ICF and $1n$ transfer channel. At higher energies, the measured cross section of formation

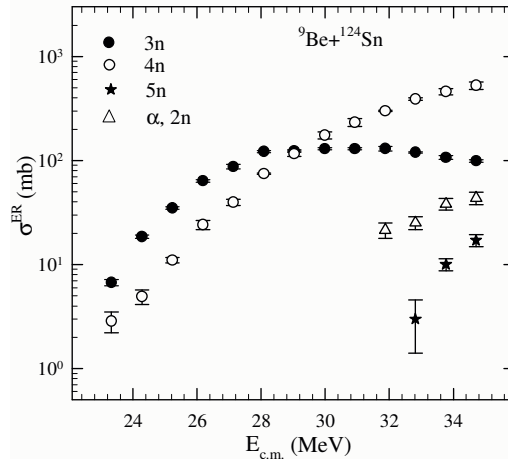


FIG. 9: Experimental ER cross sections for 3n, 4n, and 5n evaporation from CF are represented by filled circles, open circles, and filled stars, respectively. Open triangles correspond to cross sections for 2n evaporation from the ICF generated by the capture of α by the target.

of ${}^{126}\text{Te}(\text{ICF}; \alpha, 2n)$ is about 8%. An experiment is planned to estimate the other dominant channels ${}^{127}\text{Te}(\text{ICF}; \alpha, n)$ and ${}^{125}\text{Sn}(1n$ transfer) causing the loss of flux. Measuring the energy of the charged particle ejectile along with the large clover array in these reactions will help in selecting the excitation energy of the ERs for spectroscopy beyond yrast states.

5. Implementation of Digital Data Acquisition System for the Clover Array and the Ancillary Detectors

The clover array is designed for 24 Compton suppressed clover detectors arranged in a spherical geometry with 6 detectors at 90° and 3 detectors each at 23°, 40°, 65°, 115°, 140° and 157° with respect to the beam direction. The distance from the target to crystal is 25 cm and the overall photo-peak efficiency is around 5% at $E_\gamma \sim 1$ MeV. A PCI-PXI based digital data acquisition (DDAQ) system with 112 channels has been implemented for this array using Pixie-16 module by XIA LLC as shown in Fig. 10. The logic signal is generated



FIG. 10: The picture of the digital data acquisition system for the 24 Compton suppressed Clover array and the ancillary detectors.

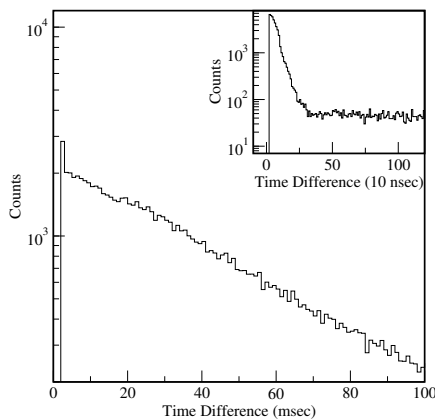


FIG. 11: The time stamp difference between any two consecutive events in an in-beam experiment for $^{28}\text{Si} + ^{165}\text{Ho}$ reaction at 158 MeV.

for each BGO anti-Compton shields through conventional fast trigger circuits using time filtering amplifier (TFA) and constant fraction discriminator (CFD). This signal is given to the respective Pixie-16 modules for the veto. The DDAQ is to provide good energy and timing resolution for all 96 channels of clovers vetoed with the BGO shields operating at 12 kHz count rate for each crystal. Each channel of the DAQ digitizes the preamplifier signal of the clovers at 100 MHz sampling speed with a 12 bit FADC. Fast filter (FF) trigger is generated once the fast filter pulse crosses the threshold. In absence of veto from the respective BGO shield, FF trigger generates a validate signal. It can operate both in triggerless as well as multi-fold coincidence mode. For each valid preamplifier pulse, energy is obtained by on-board digital processing of the pulse shape and the arrival time is obtained by latching the clock with the valid trigger. The coincident events are identified by looking at the time stamps for different channels. The time difference between consecutive events in different channels is shown in Fig 11. The initial peak shown in the inset indicates the coincident events in the in-beam experiments. Each preamplifier pulse above the threshold defines an event in the present system. The time stamp of each event was plotted against the event number in Fig 12. The events with small time difference as marked in Fig 12 are in coincident. Thus each channel produces individually time stamped events assembled into data buffers for each module. Digital system is synchronized for all the modules with the precision given by that of the clock. It has also the capabilities to couple other ancillary detectors like NaI(Tl) gamma ray multiplicity filters and CsI(Tl)/Si charged particle detectors with the clover array. One and multi-fold data has been acquired with different radioactive sources and beam induced reactions for testing of this system for coincidence measurements, energy and timing resolution studies for the clovers. A peak-to-total ratio of $\sim 40\%$ has been achieved with the Compton suppression for ^{60}Co source in the add-back mode. The full width at half maximum for

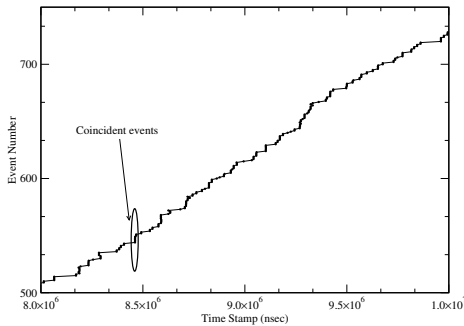


FIG. 12: The timestamp *vs.* event number plot for the in-beam experiment with 14 clover detectors.

1408 keV transition is found to be 1.96 keV. Trapezoid filter parameters are optimized for high count rate experiments up to 20 kHz to get a maximum FWHM of ~ 2 keV at 1.33 MeV. The time resolution was found to $\sigma_{rms} = 5$ nsec with coincident measurement with one crystal of the clover and BaF₂ detector for ⁶⁰Co. This is obtained by storing the trace of the pulses of clover and doing off-line analysis with CFD algorithms. A typical in-beam spectrum with gate on 287 keV transition of ¹⁸⁵Au is shown in Fig. 13. The existing level scheme of ¹⁸⁵Au [33] is verified with the data taken with the new DDAQ. This confirms the successful commissioning of the DDAQ. The deadtime of the system was estimated to be less than 1% for 50 channels each counting at 3 kHz rate in trigger less mode.

6. Conclusion

Coupling of the DDAQ with the clover array will give the opportunity to handle optimum count rate for gamma-gamma coincidence data. This will facilitate the investigation of high spin states to probe wide variety of phenomena like anti-magnetic rotations, chiral rotations, chopstick mode and tetrahedral shape in different nuclei. In addition, an array of charged particle detectors are planned to be coupled with the Clover array. This ancillary detector array along with the DDAQ will provide new capability of the clover array for the channel selection in different nu-

clear reactions for high spin spectroscopy, nuclear structure study of heavy nuclei through alpha-decay tagging with short $T_{1/2}$, search of isomers and reaction dynamics study in case of deuteron, tritium and alpha breakup of the weakly bound nuclei.

Acknowledgments

This work results from collaborative efforts. I'd like to thank my colleagues A.Y. Deo, Z. Naik, T. Trivedi, V.V. Parkar, S. Sihotra, S. Kumar, S. Sharma, S. Saha, J. Sethi, B. S. Naidu, P.B. Chavan, S. Jadav, R. Donthi, P. K. Joshi, P. Verma, S. Sinha, S. Santra, D. Mehta, G.H. Bhatt, J. Sheikh, Y. Sun, A.K. Jain, R.K. Bhowmik, H.C. Jain, and all the members of INGA collaboration. The support of the accelerator staff of Pelletron Linac Facility at Mumbai and IUAC, New Delhi during the experiment is acknowledged.

References

- [1] E. S. Paul *et al.*, Phys Rev. C **71** (2005) 054309.
- [2] P. Mason *et al.*, Phys. Rev. C **72** (2005) 064315.
- [3] C. M. Petrache *et al.*, Phys. Lett. **387 B** (1996) 31.
- [4] S. Lakshmi *et al.*, Nucl. Phys. **A 761** (2005) 1.
- [5] S. Kumar, R. Palit, *et al.*, Phys. Rev. C **76** 014306 (2007).
- [6] S. Sihotra *et al.*, Phys. Rev. C **78** (2008) 034313.
- [7] A.Y. Deo, R. Palit, *et al.*, Phys. Rev. C **79**, 067304 (2009).
- [8] P. Fallon, Nucl.Phys. **A 752**, 231c (2005).
- [9] A.J. Simons, *et al.*, Phys.Rev. C **72**, 024318 (2005).
- [10] S. Roy, *et al.*, Phys. Lett. **B** *in press*.
- [11] R. Palit, *et al.*, Nucl. Phys. **A834**, 81c (2010).
- [12] A. Gade *et al.*, Nucl. Phys. **A 673** (2000) 45.
- [13] W. F. Mueller *et al.*, Phys. Rev. C **73** (2006) 014316.
- [14] A. Jungclaus *et al.*, Phys. Rev. C **77** (2008) 024310.

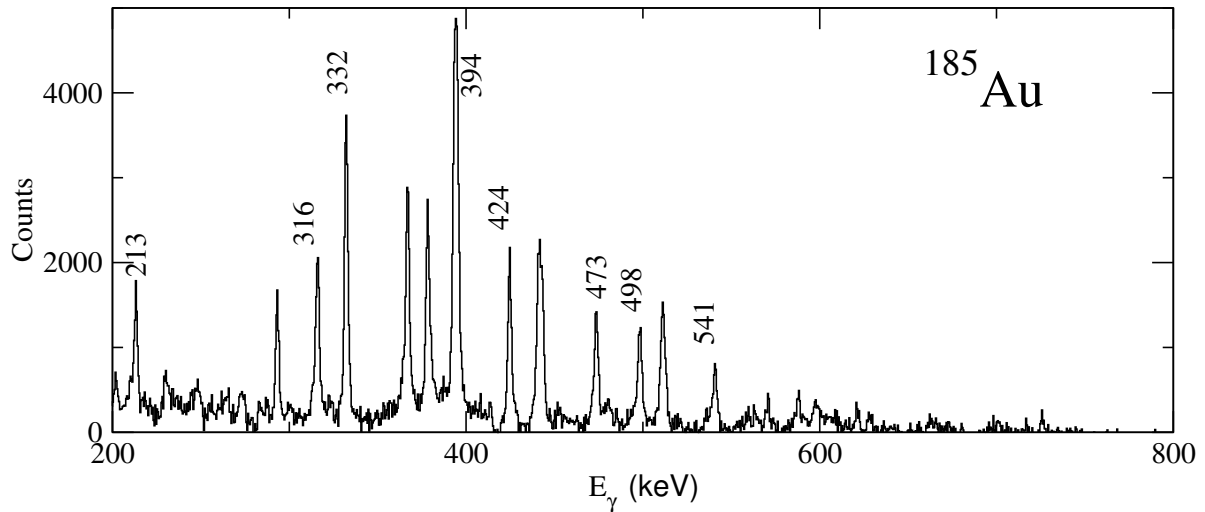


FIG. 13: The 287 keV gated gamma spectrum obtained from the time stamp list mode data recorded in the DDAQ showing the transitions of ^{185}Au produced in $^{28}\text{Si} + ^{165}\text{Ho}$ at 158 MeV beam energy.

- [15] T.R. Saito, *et al.*, Phys. Lett. **B 669** (2008) 19.
- [16] S. Frauendorf, and J. Meng, Nucl. Phys. **A617**, 131 (1997).
- [17] K. Higashiyama, N. Yoshinaga, and K. Tanabe, Phys. Rev. C **72**, 024315 (2005).
- [18] K. Starosta, *et al.*, Phys. Rev. Lett. **86**, 971 (2001).
- [19] A.Y. Deo, *et al.*, Phys. Rev. C **73** 034313 (2006).
- [20] J. Meng, *et al.*, Phys. Rev. C **73** (2006) 037303.
- [21] S. Sihotra, *et al.*, Eur. Phys. J. A **43**, 45 (2010).
- [22] Zashmir Naik, C. R. Praharaj, Phys. Rev. C **67**, 054318 (2003).
- [23] P. Joshi, *et al.*, Phys. Rev. Lett. **98** 102501 (2007).
- [24] F.R. Espinoza-Quinones, *et al.*, Phys Rev. C **52** 104 (1995).
- [25] C.-Y. He, *et al.*, Nucl. Phys. **A834**, 84c (2010).
- [26] E.A. McCutchan, Dennis Bonatsos, N.V. Zamfir, and R.F. Casten, Phys. Rev. C **76**, 024306 (2007).
- [27] E.Grodner, *et al.*, Phys. Rev. Lett. **97**, 172501 (2006).
- [28] S.Mukhopadhyay, *et al.*, Phys. Rev. Lett. **99**, 172501 (2007).
- [29] L.Goettig, *et al.*, Nucl.Phys. **A357**, 109 (1981).
- [30] J.A. Sheikh, *et al.*, Nucl.Phys. **A824**, 58 (2009).
- [31] A.Zemel, *et al.*, Nucl.Phys. **A383**, 165 (1982).
- [32] V.V. Parkar, *et al.*, Phys. Rev. C **82** 054601 (2010).
- [33] A.J.Larabee, *et al.*, Phys. Lett. **B169**, 21 (1986).